Electron Capture and Loss Cross Sections of Fast Bromine Ions in Gases*

S. Datz, H. O. Lutz,† L. B. Bridwell,‡ and C. D. Moak
Oak Ridge National Laboratory, Oak Ridge, Tennessee 37830
and
H. D. Betz§ and L. D. Ellsworth
Kansas State University, Manhattan, Kansas 66504
(Received 2 February 1970)

Br ions with energies of 13.9 and 25 MeV from the Oak Ridge tandem accelerator have been used to measure ionic charge-state distributions in dilute gas targets of H_2, He, and Ar. A least-squares technique has been developed to obtain complete sets of electron charge-exchange cross sections from any number and range of measured nonequilibrium charge distributions. Characteristic irregularities, which originate in the atomic shell structure of the Br ions, have been found in the cross sections for capture of a single electron. Multiple electron capture and loss, as well as equilibrium charge distributions, are discussed.

I. INTRODUCTION

In recent years the study of the interactions of fast heavy ions with matter has received appreciable attention. Of particular interest is the process of electron capture and loss. Measurements of charge-exchange cross sections for light ions up to argon, inclusive, have been reported in detail,[1] but only limited information is available for heavier ions. As theoretical attempts to calculate cross sections have proven to be extremely difficult, extended experimental data are vital not only for matters of practical interest but also for an improved understanding of the rather complicated charge-changing collisions. In this experiment, nonequilibrium charge distributions have been measured for 13.9- and 25-MeV ^{79}Br ions traversing gas targets of various thicknesses of H_2, He, and Ar. A new method of analysis has been developed to determine the cross sections of significant influence from any range of nonequilibrium charge distributions which have been measured for a given energy of the ion and a given target material.

The results provide information about consistent sets of cross sections for capture and loss of one or more electrons. The dependence of the capture cross section values on the ionic charge reveals the influence of atomic shell structure in heavy ion collisions and indicates the insufficiencies of present statistical models for charge-changing collisions.

When ions of charge q collide with neutral target atoms or molecules, they may capture or lose one or more electrons on each encounter. The populations Y_q of the various ionic charge states produced are given by the system of differential equations

$$\frac{d}{dx} Y_q(x) = \sum_{q'=q_i}^{q_f} \sigma_{q'q} Y_{q'}(x), \qquad q = q_i \cdots q_f, \quad \sigma_{qq} \equiv -\sum_{q' \neq q} \sigma_{qq'}, \tag{1}$$

where $\sigma_{qq'}$ is the probability in cm^2/atom (see Ref. 2) that the charge q of an ion changes to q' after the collision, and x is the thickness of the target in atoms/cm^2. Equation (1) takes into account only those collisions in which the charge of the ion is really changed, and does not include elastic collisions or encounters in which, for example, one electron is captured and lost later, perhaps because of auto-ionization, before the ion undergoes another collision or enters the analyzer. Also, collisions in which only excitation occurs are not included. It is further assumed that the total energy loss of all ions in the target is negligible and that the gas target is so dilute that the ions are in the ground state before any charge-exchange collision occurs. Therefore, all the cross sections are considered as constant. Given a set of $\sigma_{qq'}$ it is possible to evaluate the Y_q by numerical integration of Eq. (1).

II. EXPERIMENTAL PROCEDURE

The experimental arrangement is shown in Fig. 1. Single-component beams of 13.9-MeV Br^{5+} and 25-MeV Br^{8+} ions were obtained from the Oak Ridge tandem accelerator. The beam passed through a thin gas cell to produce a charge distribution. The fanning magnet then selected a single specific charge state to be used in the cross section measurements. In this way we obtained high charge purity beams (98–99%) of from 6+ to 10+ at 13.9 MeV and 7+ to 11+ at 25 MeV. These beams were

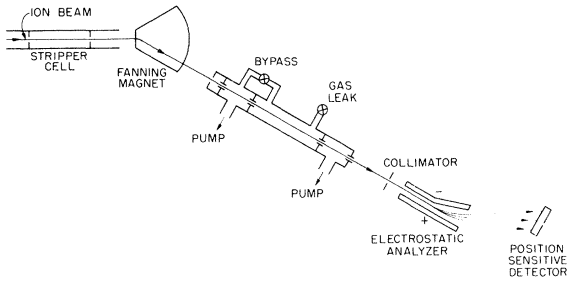

FIG. 1. Schematic experimental arrangement.

then passed through the main windowless gas cell (28 cm long), and the charge-state distributions were determined with an electrostatic analyzer and position-sensitive detector system.[3] The cell was differentially pumped through two sets of apertures. The center section was 28 cm long. The apertures were canals 2 mm in diam and 5 cm long with thin constrictions of 1 mm at the downstream ends. A pressure ratio of a factor of 10^4 could be maintained with the pumps used up to pressures of 1 Torr in the cell. Cell pressures were measured with a differential manometer (MKS instruments). The bypass valve when fully opened could be used for rapid evacuation of the cell. Probably because of outgassing, a small residual pressure buildup occurred when the bypass valve was completely closed. Since even small pressures of high cross section hydrocarbon vapors could interfere greatly with measurement of the small charge-changing cross sections in hydrogen and helium gas, it was found advantageous to keep the bypass valve slightly open during a run. This gave a pumping speed sufficient to handle the outgassing of the system and only required a slight increase in the flow rate of the target gas for the maintenance of a given pressure. The electrostatic analyzer spread the beam until the various emerging charge-state components were spatially separated. A position-sensitive detector of the silicon surface-barrier type[4] was used to detect particles in the separated beam. With a detector 2 cm in length, a position resolution of 0.2 mm was obtained (see Fig. 2). Simultaneous recording of all charge states eliminated normalization problems. With as many as ten charge states being recorded in one spectrum, typical peak-to-valley ratios of the dominant charge groups were ≥ 100. Typical spectra contained ~ 50 000 counts, so that statistical errors in all charge fractions normally were small. The width of each charge group, given by the over-all experimental resolution as well as the energy spread in the beam, was generally much smaller than the spacing between adjacent groups. Charge-state distributions were obtained as a function of pressure with He, H_2, and Ar target gases. Purities of He and Ar were 99.99%. The electrolytically produced hydrogen gas was passed through a "deoxo" filter and a liquid-nitrogen-cooled trap to remove oxygen and water vapor impurities. Distribution sets were obtained at 13.9 MeV for initial charges 6+, 7+, 8+, and 10+ in H_2, and 6+, 8+, and 10+ in He and Ar. At 25 MeV distributions were obtained with beams of 7+ through 11+ in H_2; 7+, 8+, 9+, and 11+ in He; 7+ and 9+ in Ar.

III. METHOD OF ANALYSIS

A. Slope Method

The slope method has been widely used[1,5-8] for determining charge-exchange cross sections from the linear range of the nonequilibrium distribution curves, in which mainly single-collision events occur. Because of the limitations discussed below, this method has been applied in these calculations only to determine approximate values of some of the cross sections.

If the determinations are based solely on the

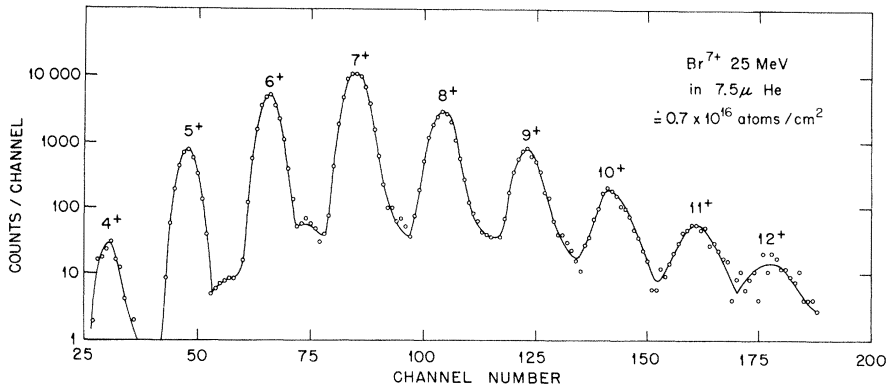

FIG. 2. Typical charge-state spectrum as obtained from the position-sensitive solid-state detector system.

slope method, three experimental conditions must be met: (i) a pure charge state k has to be selected for the incident beam, (ii) the total amount of any residual gas between the charge selector and the analyzer must be so small that its effect on the incident beam is negligible even for the smallest target thickness, and (iii) measurement of the nonequilibrium distribution has to be done with all initial charge states in the range $q_i \leq k \leq q_f (q_f - q_i \lesssim 10$ for fast heavy ions and heavy targets) if a complete set of cross sections is to be obtained. Conditions (i) and (ii) are necessary to ensure that all charge fractions increase linearly with increasing target thickness x as given by the following approximate solution to Eq. (1):

$$Y_q = \sigma_{kq}\, x \quad (k \neq q). \tag{2}$$

But even if conditions (i) and (ii) are fulfilled, the relative values of the cross sections may be such that the linear range for some charge states is too small for an accurate determination of the slope as defined by Eq. (2). Appreciable deviations from linearity already occur at a target thickness where the fraction Y_k of the incident beam may still be more than 90%. Consequently, a straight-line fit may easily introduce errors of 10–20% in the determination of a single-capture cross section $\sigma_{k,k-1}$. In case of small double-capture cross sections $\sigma_{k,k-2}$, however, considerably larger errors, in the order of 100%, are possible. As a rule rather than an exception, the fraction Y_{k-2} will be populated not only by double-capture $Y_k \rightarrow Y_{k-2}$, but also by two single-capture processes $Y_k \rightarrow Y_{k-1} \rightarrow Y_{k-2}$. Neglect of these processes causes an overestimate of $\sigma_{k,k-2}$.

Another serious disturbance arises from any residual gas, especially if its cross sections differ appreciably from those of the target gas. Equation (2) is then invalid for $x \rightarrow 0$ as the distribution is not linear; in fact, the population of some charge fractions may actually decrease for very small values of x before the major increase occurs. It is important to note that condition (ii) is not equivalent to the single-collision condition which is a necessary but not sufficient condition for obtaining linear slopes in the presence of residual gas.

A more accurate determination of cross sections usually requires that several corrections be made to Eq. (2), as well as for the appreciable decrease of Y_k in the linear region.[5] Finally, certain iteration procedures have to be used.[1] In most of our experiments the observed slopes showed significant deviations from linearity, even when the residual gas reduced the intensity of the initial population by less than 4%. Moreover, in all cases the nonequilibrium distributions have been measured nearly up to equilibrium. A more comprehensive determination of the cross sections, therefore, as well as the use of the full information which is contained in the experimental data, required the development of a different method of analysis.

B. Least-Squares Method

The least-squares method to be described[9] allows an efficient determination of cross sections from any part of the nonequilibrium distributions, provided that a sufficient number of charge fractions differ from the equilibrium distribution. Of course, the linear range may also be included. In contrast to the slope method, the initial conditions for $Y_q(x_0)$ are not restricted and linear slopes are not required. Residual gas outside the target cell is not disturbing, and, if intermixed with target gas, it does not introduce complications as long as its contributions to charge-exchange effects are negligible at the end of the linear range. In this case, the residual gas acts as if it were located in front of the target cell and serves only to modify the initial charge fractions $Y_q(x_0)$ in the range of single collisions; its contributions can be neglected for greater target thicknesses.

In the single-collision range, good information may be obtained even for a few extremely small multiple capture and loss cross sections σ_{kq}. The nonlinear range at increased x reflects mainly the interaction of the larger cross sections $\sigma_{qq'}$, where q is different from the incident charge state k. In general, values of cross sections over a range of 3 to 4 orders of magnitude can be determined with good accuracy, especially if the single-collision range is part of the experimental data.

For a given complete set of parameters $\sigma_{qq'}$, and given initial conditions $Y_q(x_0)$, the system of Eq. (1) can be integrated numerically. As the accuracy of the computed charge fractions must not necessarily be better than ~0.1% a simple Runge-Kutta integration may be employed. This procedure yields the full nonequilibrium distribution including charge equilibrium, and comparison with the measured fractions can be made. The most straightforward method of determining the constants $\sigma_{qq'}$ in Eq. (1) is a least-squares fit of the experimental distribution; i.e., one has to minimize the square sum

$$S = \sum_{m=1}^{m_0} W_m\, (Y_m - Z_m)^2 . \tag{3}$$

Here, Y_m and Z_m are the experimental and calculated charge fractions, respectively, and W_m are the weighing factors chosen with respect to the experimental uncertainties of Y_m and x_m. The index m covers all nonzero charge fractions which have been measured for all charge states, target

thicknesses x_m and different nonequilibrium distributions belonging to the same cross section set. For convenience, all unknown cross sections $\sigma_{qq'}$ are arranged as a vector $\underline{\sigma}$ with the components σ_n, where $n = 1, \ldots, n_0$. A change $\Delta\underline{\sigma}$ of the n_0 cross sections then causes certain changes ΔZ_m of the calculated fractions and consequently S will vary; with $\Delta Y_m = Y_m - Z_m$ we obtain

$$S + \Delta S = \sum_{m=1}^{m_0} W_m (\Delta Y_m - \Delta Z_m)^2 \quad . \tag{4}$$

Minimization of a square sum is a well-known technique extensively described under general aspects[10,11] as well as for special applications.[12] The least-squares analysis is extremely simple if the square sum S is a linear function of the unknown parameters. In the present case, however, the dependence $\Delta Z_m(\Delta\sigma_n)$ is nonlinear and implicit. Thus the following linearization becomes necessary:

$$\Delta Z_m = \sum_{n=1}^{n_0} A_{mn}\, \Delta\sigma_n \, . \tag{5}$$

All coefficients $A_{mn} = \partial Z_m/\partial\sigma_n$ can be calculated by means of n_0 numerical integrations of the system (1). If we insert (5) in (4), the minimum condition $\partial(S + \Delta S)/\partial\sigma_n = 0$ yields the desired changes of the cross sections:

$$\Delta\underline{\sigma} = [\underline{A}^T \underline{W} \underline{A}]^{-1} \underline{A}^T \underline{W}\, \Delta\underline{Y} \quad . \tag{6}$$

In (6), the elements A_{mn} and W_m form a rectangular $m_0 \times n_0$ and a diagonal $m_0 \times m_0$ matrix, respectively, and the components ΔY_m are arranged as a vector $\Delta\underline{Y}$. The matrix $\underline{A}^T \underline{W} \underline{A}$ is of full rank n_0 and can be inverted with standard routines.

As Eq. (5) is only a first-order approximation, the new recalculated squares sum will not be the smallest sum $S_{\min}$ which is possible. The proximity of S to $S_{\min}$ is tested, for example, by comparing the actually resulting decrease ΔS with the anticipated decrease ΔS_{lin} as obtained from the linear model (5); thus

$$\Delta S_{\text{lin}} = -\, \Delta\underline{Y}^T \underline{W} \underline{A}\, \Delta\underline{\sigma} \quad . \tag{7}$$

The closer the actual S approaches $S_{\min}$, the smaller becomes the difference between ΔS and ΔS_{lin}. Thus, in order to obtain $S_{\min}$, the whole procedure is to be repeated one or more times. In general, however, the convergence is rapid, although as many as 50 cross sections may be involved. The necessary number of iteration steps depends, of course, mainly on the initial cross section set. But the deviations from the linear relation Eq. (5) are usually so small that more than one iteration step becomes necessary only if the initial cross sections differ more than about 50% from the best values. In any case, the obvious absence of physical secondary minima causes a very fast and direct convergence of all cross sections.

For an effective and most comprehensive cross section analysis, it is imperative not only to decide what cross sections should be included in the system Eq. (1), but also to know how meaningful are the resulting cross section values. Therefore, knowledge is required about determinate errors $\delta\sigma_n$ associated with the best-fit values σ_n which may differ by many orders of magnitude.

We can assume that all uncertainties $\delta\sigma_n$ arise from the errors δY_m of the measured fractions. All errors δx_m of the target thickness must be included in δY_m. If we employ the standard definition of the weights $W_m = \delta Y_m^{-2}$ and neglect the correlation between the uncertainties δY_m, the desired errors of the resulting cross sections are given by

$$\delta\sigma_n = [(\underline{A}^T \underline{W} \underline{A})^{-1}_{nn}]^{1/2} \quad . \tag{8}$$

Even if the statistics and the repeatability of the data give only rough effective uncertainties $\delta\underline{Y}$, Eq. (8) is useful enough to decide, for example, whether a specific cross section remains practically undetermined or not. This selection of cross sections is done automatically by the computer program.

The confidence in the errors $\delta\sigma_n$ can be tested by a comparison between the resulting least-square sum $S_{\min}$ and the theoretical residual S_R. With the above definition of the weights, a deviation of the calculated fraction from the experimental charge fraction just within the error ($\Delta Y_m = \delta Y_m$) gives a contribution of 1 to the square sum. Then, the least-squares theory predicts a residual $S_R = m_0 - n_0$. For a proper choice of the uncertainties δY_m, we should obtain $S_{\min} \approx S_R$ and, consequently, Eq. (8) should give the most probable cross section errors. Systematic errors, of course, are not included. On the other side, significant differences between $S_{\min}$ and S_R suggest a correction of the initial uncertainties δY_m:

$$\delta Y_{m|\text{corr}} = \delta Y_m [S_{\min}/(m_0 - n_0)]^{1/2} \, . \tag{9}$$

This correction in turn causes an adjustment of $\delta\sigma_n$ by the same factor and the final average errors $\delta\sigma_{n|\text{corr}}$ should be quite reliable.

IV. RESULTS AND DISCUSSION

Three of the measured population growth curves are presented in Figs. 3–5 for Br ions in H_2 and Ar at 13.9 MeV and in He at 25 MeV. The normalized fractions Y_q of the charge state q are plotted versus the thickness X of the target gas. For a better demonstration of the range in X and Y a double logarithmic scale was chosen. The solid

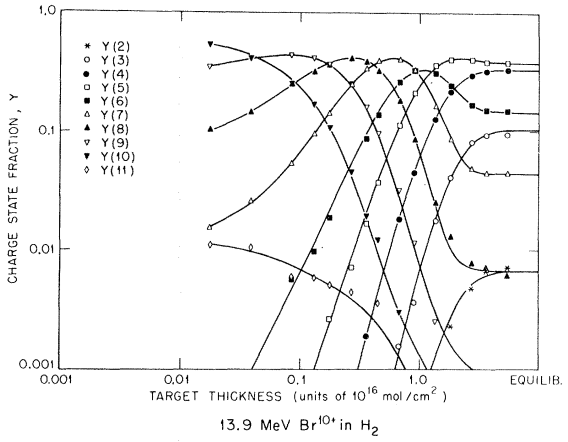

FIG. 3. Charge-state fraction for 13.9-MeV Br^{10+} ions in H_2 as a function of target thickness. The plotted curves are obtained from a calculation using the complete set of cross sections obtained from this data and from similar data using initial charge states 6+, 7+, and 8+.

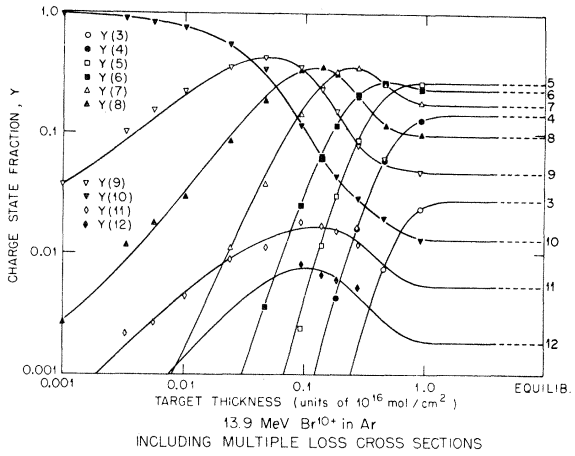

FIG. 5. Charge-state fraction for 13.9-MeV Br^{10+} ions in Ar as a function of target thickness. The plotted curves are obtained from a calculation using the complete set of cross sections obtained from these data and from similar data using initial charge states 6+ and 8+.

lines represent the charge fractions calculated with the corresponding best cross section set obtained from the least-squares analysis of all measured distributions. In general, data points are approximated quite well except in the case of a few low-intensity fractions. It is obvious from Figs. 3–5 that the increase of charge fractions at small X generally shows deviations from linearity.

Although it is expected that in principle multiple electron loss and capture processes occur, it is interesting to see how much these processes influence the nonequilibrium distributions. In Fig. 6, an additional best-fit calculation was made for the same distribution as shown in Fig. 5, but only cross sections for single capture and loss were used. Since the initial charge state $k = 10+$ is much higher than the mean ionic equilibrium charge $\bar{q} = 6$, electron capture processes are dominant; for example, the ratio for capture and loss probability for the incoming charge state Y_{10} is

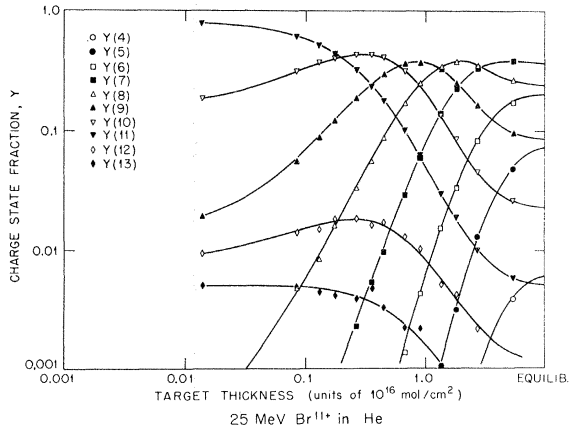

FIG. 4. Charge-state fraction for 25-MeV Br^{11+} ions in He as a function of target thickness. The plotted curves are obtained from a calculation using the complete set of cross sections obtained from this data and from similar data using initial charge states 7+, 8+, and 9+.

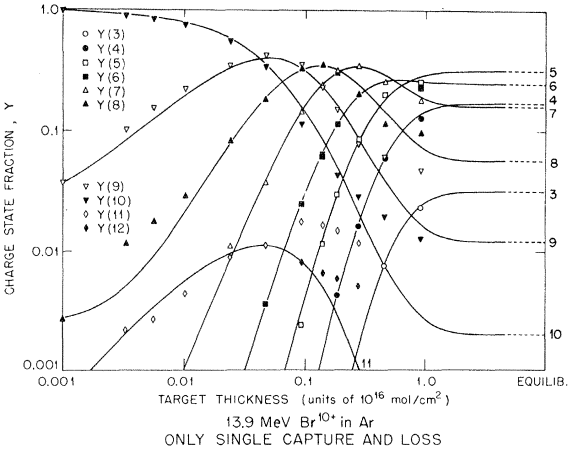

FIG. 6. Population curves calculated to fit the data given in figures but omitting multiple loss cross sections. Note that the population of 12+ predicted in this way lies below the range of the graph.

62:1. Nevertheless, comparison between Figs. 5 and 6 indicates that, without taking multiple electron losses into account, no satisfactory analysis for cross sections can be done. The disagreement is obvious especially for the charge states Y_{11} and Y_{12} with $q > k$, which are populated mainly by loss of charge state Y_{10}. In the case of lower incoming charge states, test fits with the restricted cross section set are even worse.

Single-electron capture. Figure 7 shows the resulting cross sections for capture of a single electron versus the charge state at 13.9 MeV. Most single-capture cross sections could be determined with very high accuracy, partly – as noted above – because they have the strongest influence on the nonequilibrium distributions, partly because double capture turned out to be unlikely.

As expected, single-capture probabilities $\sigma_c(q)$ increase with the charge state q, but in all cases characteristic anomalies were found which were clearly outside the limits of error. Compared with a smooth trend in $\sigma_c(q)$, the cross sections $\sigma_c(6)$ and to some extent $\sigma_c(8)$ are above the trend, whereas $\sigma_c(7)$ is clearly below. In fact, in all cases (see Fig. 7), $\sigma_c(7)$ is smaller than $\sigma_c(6)$. Figure 8 shows the ionization potentials calculated for bromine by Carlson *et al.*[13] using Hartree-Fock wave functions as a function of ion charge state. In bromine ions with charge $q = 5$, all five $4p$ electrons are removed. The slight inflection from $q = 5$ to $q = 7$ corresponds to removal of the two $4s$ electrons and the jump at $q = 8$ corresponds to removal of the first electron from the $3d$ shell.

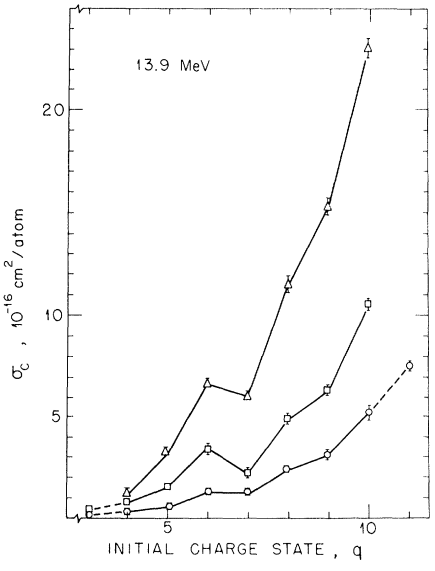

FIG. 7. Single-capture cross sections for 13.9-MeV Br ions in Ar △, He □, and H_2 ○.

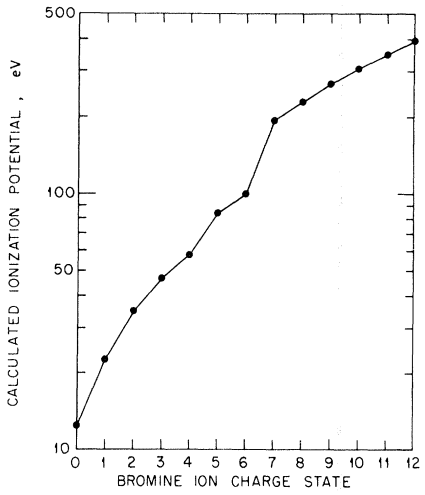

FIG. 8. Calculated single-ionization potentials for Br ions as a function of initial charge states (courtesy of T. A. Carlson and C. W. Nestor, Jr.).

One might then use quasichemical reasoning and attribute the high value of $\sigma_c(6)$ to closing the $4s$ subshell, the value of $\sigma_c(7)$ to beginning a new subshell, and the high value of $\sigma_c(8)$ to closing the $3d$ subshell. With this reasoning, however, one would certainly expect the largest effect to have occurred at $\sigma_c(8)$. On the basis of energetics and of density states, one might expect capture to occur principally to highly excited levels of the lower-charge-state ion. This effect would tend to blur any clear-cut shell boundaries in electron capture. An alternative explanation can be made if one proposes the necessity for small excitation of a bound electron to stabilize electron capture. In this case the availability of a $4s$ electron enhances the $\sigma_c(6)$, while the necessity for exciting an electron out of a closed shell depresses $\sigma_c(7)$. In any case, a more detailed knowledge of the actual capture process is required in order to fully understand the shell effects observed in the cross sections.

Another question of interest is the over-all dependence of the single-capture cross sections σ_c on the charge q of the ions and the nuclear charge Z_{med} of the target gas. As can be seen from Figs. 9 and 10, where σ_c is plotted versus q in a log-log scale, the smoothed increase of σ_c may be approximated by a power function

$$\sigma_c(q) \sim q^{\bar{\alpha}} \quad , \tag{10}$$

where the average exponent $\bar{\alpha}$ is close to 3 and 4 at 13.9 and 25 MeV, respectively. Our data indicate no systematic dependence of $\bar{\alpha}$ on q. Also, the target gas does not seem to have a strong influence on $\bar{\alpha}$. Measurements with light ions re-

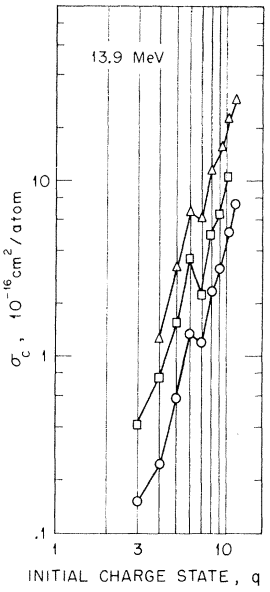

FIG. 9. Log-log plot of single-capture cross sections for 13.9-MeV Br ions in Ar △, He□, and H_2○.

sulted in values of α ranging from 1.5 to 3, but stronger powers can not be ruled out; an increase of α with velocity v of the ions was also observed.[5,6] Theoretical calculations lead to the same proportionality Eq. (10), where the predictions, depending on the model, are $\bar{\alpha}=2$ (Refs. 1, 14, 15) or $\alpha=3$ (Refs. 1, 16). Recent experiments with iodine ions in nitrogen,[7] however, indicate a strong dependence of α on q: for values of q smaller than the mean ionic charge at equilibrium $\bar{q}$, $\bar{\alpha}$ decreases rapidly as q is increased but seems to reach the constant value $\bar{\alpha}=2$ for $q \gtrsim \bar{q}$. For the dependence of σ_c on the medium, no clear relationship can be found from our data. For a given q, average ratios of σ_c in H_2, He, and Ar are 1: 2. 5: 5 and 1: 3: 10 at 13. 9 and 25 MeV, respectively. If one doubles the values for H_2, which corresponds to a change of the cross section units to cm^2/molecule, the 13. 9-MeV ratios come close to the theoretical dependence $\sigma_c \propto Z_{\text{med}}^{1/3}$ (Ref. 15), but the 25-MeV ratios still cannot be reconciled.

Single-loss cross sections and multiple electron loss. Figure 11 shows cross sections for single loss at 13. 9 and 25 MeV in H_2, He, and Ar. A direct ion-electron impact treatment of the single-electron-loss problem seems realistic for light target gases. Within a shell, $\sigma_L(q)$ is expected to be proportional to the number of electrons n_i of the same ionization potential remaining in the shell.[1] This prediction holds well for H_2 and He target atoms in the +3 to +7 ($n=4$) region; for example, $\sigma_L(q)/n_i$ is equal to 0.10 ± 0.01 for Br ions in H_2 in the range $3 \leq q \leq 7$ and $0.26 \pm .02$ for He. This reasoning does not seem to extend to the +8 to +11 region, perhaps because the ion velocities lie below the orbital velocities in the 3*d* shell. With respect to the errors of the loss cross sections, no significant shell effects can be seen. In the case of Ar at 13.9 MeV, there is a discontin-

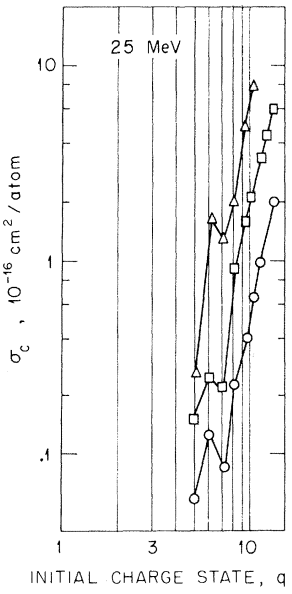

FIG. 10. Log-log plot of single-capture cross sections for 25-MeV Br ions in Ar△, He□, and H_2○.

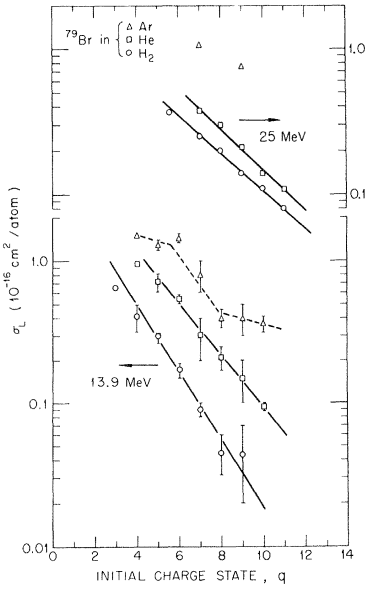

FIG. 11. Single-electron-loss cross sections for 13.9- and 25-MeV Br ions in Ar △, He □, and H_2 ○.

TABLE I. Values of multiple capture and loss cross sections relative to single capture and loss. The variations shown refer to the entire range of charge states. (Multiple loss decreasing with increasing q.)

		$(\sigma_{q,q-n}/\sigma_{q,q-1})$ (%)	$(\sigma_{q,q+n}/\sigma_{q,q+1})$ (%)		
E(MeV)	Target	$n=2$	$n=2$	$n=3$	$n=4$
13.9	H_2	$\lesssim 1.0$	6-20	1-4	< 1
	He	$\lesssim 1.5$	10-25	4-8	$\lesssim 2$
	Ar	$\lesssim 3.0$	40-60	25-40	$\lesssim 25$
25	H_2	$\lesssim 0.2$	5-10	2-4	< 2
	He	$\lesssim 0.2$	10-20	4-10	< 4
	Ar	$\lesssim 5.0$	30-50	15-30	< 15

uity at $q = 9$ and 10; these two cross sections are above the established trend and this effect is not understood.

Table I lists the range of percentages of the cross sections for multiple electron capture and loss, relative to the corresponding cross sections for single capture and loss which are taken as 100%. At both energies, double capture is very small in H_2 and He, and somewhat larger in argon. This is understandable because the heavier argon atom offers more electrons for the capture process. In all cases, multiple loss is much more significant, and, for example, in argon the probability for simultaneous loss of two electrons in one encounter may reach 60% of the probability for single loss. The multiple-loss cross section decreases with increasing charge state (H_2, He). For example, the double to single loss ratio varies from 20% at charge 4+ to 6% at charge 9+ for 13.9-MeV ions in H_2. These values are considerably larger than those observed for light ions.[17] Simultaneous loss of more than four electrons certainly exists, especially in heavier strippers such as argon, but due to the limitations discussed in Sec. III, our data did not allow accurate determinations of those values. Multiple-electron-loss processes have been extensively studied in large-angle scattering of heavy ions at lower energies and will certainly contribute in a major way to the total cross section at higher energies. The best explanation of these multiple-ionization events[18] involves the formation of pseudomolecular states which dissociate into excited ions. These ions may lose inner-shell electrons, and then be multiple ionized by Auger decay. This process will be predominant for heavy ions in heavy target atoms where shell-shell overlap is important and will be less important for light target atoms. This has already been demonstrated experimentally at higher beam energies for iodine ions.[3]

Equilibrium distributions. The best least-squares fits calculated with the final cross section sets are usually very good approximations to the experimental nonequilibrium distributions. Therefore, one may expect a close prediction of equilibrium distributions which have not been measured directly. Figure 12 shows these charge distributions which have been calculated for equilibrium conditions by means of the best determined cross section sets. The distributions in He and Ar at 13.9 MeV clearly show the influence of shell effects. Charge state 6+ with one electron in the N shell is about 20% smaller than one would expect from a smoothed distribution. At 25 MeV, Y_6 lies on the slope where irregularities cannot be seen as easily as close to the top of the distribution. The same shell effect we find in our data is also observable in the equilibrium distribution of bromine ions in argon at the slightly higher energy of 15 MeV.[3]

All equilibrium distributions shown in Fig. 12

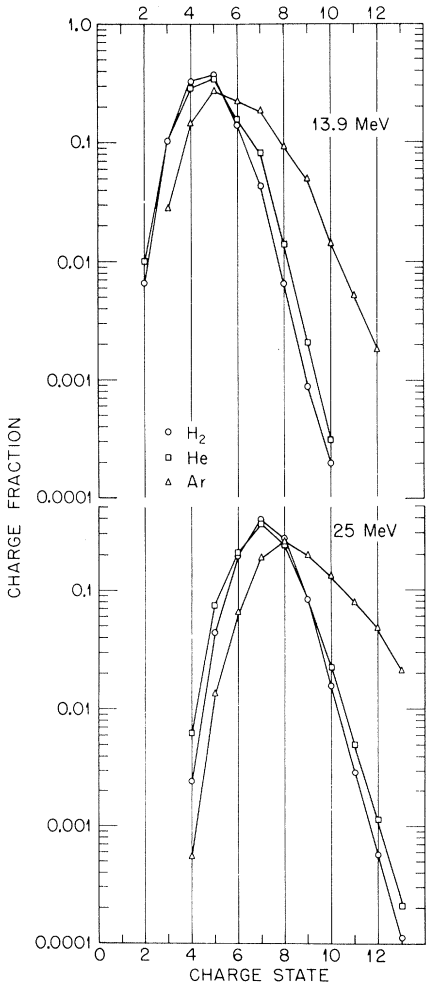

FIG. 12. Equilibrium charge-state distributions for 13.9- and 25-MeV Br ions in Ar, He, and H_2.

are asymmetrical even if the shell effect at charge state 6+ is not weighted. Especially at 25 MeV, the left-hand sides of the distributions show a sufficient number of charge fractions and fit perfectly to a Gaussian. But the charge-state populations on the right-hand side decrease much more slowly and show systematic deviations from a Gaussian, which are strongest for the distribution in argon. For the cases reported here, this asymmetry is caused by the influence of the multiple-loss cross sections which are much larger in argon than in helium or hydrogen. If these cross sections are omitted from the calculation, a more symmetric distribution is obtained. From studies of equilibrium distributions of bromine and iodine in many gas targets,[3] it is also clear that most gases resemble Ar in their stripping behavior for fast heavy ions rather than helium or hydrogen. On the other hand, equilibrium distribution asymmetries do not necessarily result from multiple-loss processes. For example, symmetrical distributions were obtained for sulfur ions stripped in gases even though a double electron loss of almost 30% was present.[19]

The mean ionic charge states $\bar{q} = \sum_q Y(q)$, calculated for our equilibrium distributions as shown in Fig. 12, are 4.7, 4.8, and 6.0 at 13.9 MeV, and 7.2, 7.1, and 8.6 at 25 MeV in H_2, He, and Ar, respectively. These average charges are larger than the most probably charge states q defined at the maximum of the smoothed charge distributions. In H_2 and He we find that $\bar{q}$ exceeds q by 0.1, whereas in argon $\bar{q} - q$ is 0.6. These values of $\bar{q}$ are in reasonable agreement with other experimental results and semiempirical predictions.[19–22] It should be noted, however, that experimental results on equilibrium distributions as well as on cross sections may be affected by energy loss, charge-dependent scattering, and stripping from excited states[23,24] in the target gas. The latter effect may influence the results, but not enough is yet known to estimate the lifetimes involved.

ACKNOWLEDGMENTS

The authors are indebted to B. Main and K. Halbach for their interest in the work and wish to give their thanks to R. Yourd and C. W. Nestor, Jr., for assistance in the handling of data.

---

*Research sponsored by the U. S. Atomic Energy Commission, under contract with Union Carbide Corporation, contract No. AT (11-1)-1766.

†Present address: Max-Plank-Institut für Kernphysik, Heidelberg, Germany.

‡Present address: Murray State University, Murray, Ky.

§Now with Massachusetts Institute of Technology, Cambridge, Mass.

[1]V. S. Nikolaev, Usp. Fiz. Nauk 85, 679 (1965) [Soviet Phys. Usp. 8, 269 (1965)].

[2]It is also common to use the units cm^2/molecule.

[3]C. D. Moak, H. O. Lutz, L. B. Bridwell, L. C. Northcliffe, and S. Datz, Phys. Rev. 176, 427 (1968).

[4]Nuclear Diodes, Inc., Prairie View, Ill.

[5]V. S. Nikolaev, L. N. Fateeva, I. S. Dmitriev, and Y. A. Teplova, Zh. Eksperim. i Teor. Fiz. 33, 306 (1957) [Soviet Phys. JETP 6, 239 (1958)].

[6]V. S. Nikolaev, I. S. Dmitriev, L. N. Fateeva, and Y. A. Teplova, Zh. Eksperim. i Teor. Fiz. 40, 989 (1961) [Soviet Phys. JETP 13, 695 (1961)].

[7]N. Angert, B. Franzke, A. Möller, and C. Schmelzer, Phys. Letters 27A, 28 (1968).

[8]A. Möller, N. Angert, B. Franzke, and C. Schmelzer, Phys. Letters 27A, 621 (1968).

[9]H. D. Betz, Bull. Am. Phys. Soc. 14, 100 (1969).

[10]M. G. Kendall and A. Stuart, in *The Advanced Theory of Statistics* (Griffin, London, 1958).

[11]E. Williams, in *Regression Analysis* (Wiley, New York, 1959).

[12]K. Halbach, in *Proceedings of the Second International Conference on Magnet Technology* (Oxford, England, 1967); UCRL Report No. UCRL-17436, 1967, (unpublished).

[13]T. A. Carlson and C. W. Nestor, Jr. (private communication).

[14]G. I. Bell, Phys. Rev. 90, 548 (1953).

[15]N. Bohr and J. Lindhard, Kgl. Danske Videnskab Selskab, Mat. Fys. Medd. 28, No. 7 (1954).

[16]V. S. Nikolaev, Zh. Eksperim. i Teor. Fiz. 33, 534 (1957) [Soviet Phys. JETP 6, 417 (1958)].

[17]I. S. Dmitriev, V. S. Nikolaev, L. N. Fateeva, and Y. A. Teplova, Zh. Eksperim. i Teor. Fiz. 43, 358 (1962) [Soviet Phys. JETP 16, 259 (1963)].

[18]U. Fano and W. Lichten, Phys. Rev. Letters 14, 627 (1965); W. Lichten, Phys. Rev. 164, 131 (1967).

[19]H. D. Betz, Institut für Angew. Physik, Heidelberg, Report No. UNILAC-Bericht 5, 1965, (unpublished).

[20]I. S. Dmitriev and V. S. Nikolaev, Zh. Eksperim. i Teor. Fiz. 47, 615 (1964) [Soviet Phys. JETP 20, 409 (1965)].

[21]H. D. Betz, G. Hortig, E. Leischner, C. Schmelzer, B. Stadler, and J. Weihrauch, Phys. Letters 22, 643 (1966).

[22]L. Grodzins, R. Kalish, and D. Murnick, Phys. Letters 24, 282 (1967).

[23]G. Ryding, A. Wittkower, and P. H. Rose, Phys. Rev. 184, 93 (1969).

[24]G. Ryding, H. D. Betz, and A. Wittkower, Phys. Rev. Letters 24, 123 (1970).